

Research Article

Highly Active Rare-Earth-Metal La-Doped Photocatalysts: Fabrication, Characterization, and Their Photocatalytic Activity

S. Anandan,^{1,2} Y. Ikuma,² and V. Murugesan¹

¹Department of Chemistry, Anna University, Chennai 600 025, India

²Department of Applied Chemistry, Kanagawa Institute of Technology, 1030 Shimoogino, Atsugi, Kanagawa 243-0292, Japan

Correspondence should be addressed to S. Anandan, svivekanand2002@yahoo.com and Y. Ikuma, ikuma@chem.kanagawa-it.ac.jp

Received 15 July 2011; Revised 23 September 2011; Accepted 24 September 2011

Academic Editor: Jinlong Zhang

Copyright © 2012 S. Anandan et al. This is an open access article distributed under the Creative Commons Attribution License, which permits unrestricted use, distribution, and reproduction in any medium, provided the original work is properly cited.

Efficient La-doped TiO₂ photocatalysts were prepared by sol-gel method and extensively characterized by various sophisticated techniques. The photocatalytic activity of La-doped TiO₂ was evaluated for the degradation of monocrotophos (MCPs) in aqueous solution. It showed higher rate of degradation than pure TiO₂ for the light of wavelength of 254 nm and 365 nm. The rate constant of TiO₂ increases with increasing La loading and exhibits maximum rate for 1% La loading. The photocatalytic activities of La-doped TiO₂ are compared with La-doped ZnO; the reaction rate of the former is ~1.8 and 1.1 orders higher than the latter for the lights of wavelength 254 nm and 365 nm, respectively. The relative photonic efficiency of La-doped TiO₂ is relatively higher than La-doped ZnO and commercial photocatalysts. Overall, La-doped TiO₂ is the most active photocatalyst and shows high relative photonic efficiencies and high photocatalytic activity for the degradation of MCP. The enhanced photocatalytic activity of La-doped TiO₂ is mainly due to the electron trapping by lanthanum metal ions, small particle size, large surface area, and high surface roughness of the photocatalysts.

1. Introduction

The remarkable progress of scientific technologies in recent years has made extremely high demands on semiconductor material. Photocatalysis using semiconductors has been extensively performed worldwide to find solutions to energy and environmental problems, since the discovery of “Honda-Fujishima Effect” three decades ago. Among the semiconductors, outstanding stability and oxidative power make TiO₂ the best semiconductor photocatalyst for environmental remediation and energy conversion processes [1–3]. However, the application of TiO₂ is yet limited by the fast recombination of electron-hole pairs and their wide band gap, which corresponds with UV light [4]. Therefore, the studies of modifying TiO₂ to reduce the electron-hole recombination and sensitization towards visible light have been extensively investigated. Metal ion doping has been widely performed on semiconductors to minimize electron/hole recombination and enhance their absorption towards visible light region [5–8]. For example, Choi et al. found that TiO₂ doping with Fe³⁺, Mo⁵⁺, Ru³⁺, Os³⁺, Re⁵⁺, V⁴⁺, and

Rh³⁺ increased photocatalytic activity in the liquid-phase photodegradation of CHCl₃. However, (transition metal-) doped TiO₂ suffers from a thermal instability or an increase in the carrier recombination centers [9]. Alternately, rare earth-doped metal oxides are potentially attractive materials for various optical and electronic applications because such materials exhibit unique physical and chemical properties such as fluorescence [10–12], persistent spectral hole burning [13–15], and ion conductivity [16]. Moreover, rare earth ions have radii larger than Ti⁴⁺, so they are mainly distributed on the surface when deposited onto TiO₂, that keep large surface areas of TiO₂ when treated at high temperatures. Atribak et al. [17] studied the catalytic oxidation of soot using La-modified TiO₂ and concluded that TiO₂ doped with 0.2% La exhibits best photocatalytic activity. In our previous studies, we developed La-doped ZnO photocatalysts and successfully applied for the degradation of organic pollutants in aqueous solution [18]. In the present study, we mainly focus on the synthesis of La-doped TiO₂, since the photocatalytic activity of TiO₂ was greater than ZnO. Moreover, the photocatalytic degradation of MCP using TiO₂, ZnO, La-doped ZnO, and

some of the commercial photocatalysts, carried out. Finally the photocatalytic efficiency of La-doped TiO₂, compared with above-mentioned photocatalysts. Herein we report the synthesis, characterization, and application of La-doped TiO₂ particles with series of lanthanum loading. La-doped TiO₂ prepared by sol-gel method and extensively characterized using various sophisticated techniques. Photocatalytic activity of TiO₂, La-doped TiO₂, and other photocatalysts have evaluated by the degradation of MCP in aqueous solution. Photocatalytic decomposition of MCP is of great significance from the viewpoint of practical applications because MCP is one of the organophosphorous insecticides which are widely used in agriculture and animal husbandry. Also, MCP has been identified as endocrine disrupting chemicals (EDCs) which causes serious adverse effects on humans. The most serious among them are premature ageing, congenital abnormalities, and impotence [19]. It has been observed from the experimental results that La-doped TiO₂ showed an excellent photocatalytic activity and relative photonic efficiency compared to other photocatalysts. Electron trapping by lanthanum metal ions, smaller particle size, large surface area, high porosity, and increase in surface roughness may be the reasons for the enhanced photocatalytic activity.

2. Experimental

2.1. Materials Preparation and Characterization. La-doped TiO₂ was prepared by sol-gel method using titanium tetraisopropoxide (Analytical grade, Merck Ltd., India) and lanthanum nitrate hexahydrate (La (NO₃)₃·6 H₂O) (Analytical grade, CDH, India) as titanium and lanthanum sources, respectively. The technical grade sample of monocrotophos (MCP) was received from Sree Ramcides Chemicals, India. HPLC grade acetonitrile was purchased from Merck, India. The lanthanum-doped TiO₂ samples were prepared by sol-gel method. Required amount of Ti (O-Bu)₄ was dissolved in absolute ethanol and the solution mixed vigorously in a solution containing appropriate amounts of water, acetic acid, and ethanol. Then lanthanum nitrate solution was added to the above sol to form a colloidal suspension. The resultant colloidal suspension was stirred and aged to form a gel. The gel was dried in vacuum and then ground. The resulting powder was calcined at 500°C and depending on the concentration of lanthanum nitrate; the photocatalysts were expressed in terms of weight percentage. The crystallinity of pure TiO₂ and La-doped TiO₂ photocatalysts was analyzed by X-ray powder diffraction (Model: PANalytical) with Cu-K α radiation in the scanning range of 2θ between 10 to 80°. The accelerating voltage and applied current were 40 kV and 40 mA, respectively. Data were recorded at a scan rate of 0.02° s⁻¹ in the 2θ range of 10° to 80°. The size of the crystallite was calculated from X-ray line broadening from the Scherrer equation: $D = 0.89\lambda/\beta \cos \theta$, where D is the average crystal size in nm, λ is the Cu-K α wavelength (0.15406 nm), β is the full width at half maximum, and θ is the diffraction angle. Specific surface area, pore volume, and pore diameter of the materials were determined from N₂ adsorption-desorption isotherms at 77 K by using a Belsorb

mini II sorption analyzer. Surface morphology of TiO₂ and La-doped TiO₂ photocatalysts were investigated by AFM (Digital Instruments, 3100) and FE-SEM (Hitachi, S-4800). X-ray photoelectron spectroscopy (XPS—Thermo Electron Corporation Theta Probe) equipped with ultrahigh vacuum chambers were used to evaluate the presence of elements in La-doped TiO₂ photocatalysts. Mg K-alpha X-rays (100 W) was used as the source at a takeoff angle of 5–75° and vacuum pressure of 10⁻⁶–10⁻⁷ Torr. The energy of monochromatic Mg K-alpha X-rays used for analysis is 1486.6 eV.

2.2. Photocatalytic Degradation Procedure and Analytical Methods. A cylindrical photochemical reactor setup was used as reported previously [20] for the degradation of MCP. The photocatalytic degradation was carried out by mixing 100 mL of aqueous MCP solution and 100 mg of photocatalyst. The experiments were performed at room temperature, and the pH of the reaction mixture was kept at solution pH. Before irradiation, the slurry was aerated for 30 min to reach adsorption equilibrium followed by UV irradiation at specific wavelength, 254 or 365 nm. Aliquots were withdrawn from the suspension at specific time intervals and centrifuged immediately at 1500 rpm. Then it was filtered through a 0.2 μ m millipore filter paper to remove suspended particles. The filtrate was analyzed by HPLC and TOC to find out the extent of degradation and mineralization of MCP. The concentration of MCP was analyzed by HPLC instrument (Shimadzu, Model: SPD-10A VP) with a UV-Vis detector. In the HPLC analysis, Shim-pack CLC-C8 column (5 μ m particle size, 250 mm length, and 4.6 mm inner diameter) and mobile phase of acetonitrile/water (6 : 4 v/v) were used with a flow rate of 1.0 mL min⁻¹. An injection volume of 20 μ L was used. The total organic carbon was determined by a TOC analyzer (Shimadzu, Model: 5000A) equipped with a single injection autosampler (ASI-5000). The concept of relative photonic efficiency (ξ_r) is very useful to compare catalyst efficiencies using a given photocatalyst (La-doped TiO₂) material and a given standard photocatalyst (TiO₂-Degussa P25) [21]. The relative photonic efficiency (ξ_r), was obtained by comparing the photonic efficiency of La-doped TiO₂ with that of the standard photocatalyst (TiO₂-Degussa P25). To evaluate ξ_r , a solution of MCP (40 mg L⁻¹) with a pH of 5 was irradiated with 100 mg of TiO₂ or La-doped TiO₂ for 0.5 h. Then, relative photonic efficiency was calculated based on the above experiments.

3. Results and Discussion

3.1. Characterization of Photocatalysts

3.1.1. XRD Patterns and TEM Analysis of TiO₂ and La-Doped TiO₂. XRD patterns of TiO₂ and La-doped TiO₂ are shown in Figure 1, in which the peaks marked “A” and “R” correspond with anatase and rutile phase, respectively. XRD analysis reveals that TiO₂ and La-doped TiO₂ photocatalysts was comprised of both anatase and rutile phases. The diffraction pattern of La-doped TiO₂ photocatalysts was similar to that of pure TiO₂. There are no peaks for the formation of composite metal oxides such as La₂O₃ in La-doped TiO₂. It

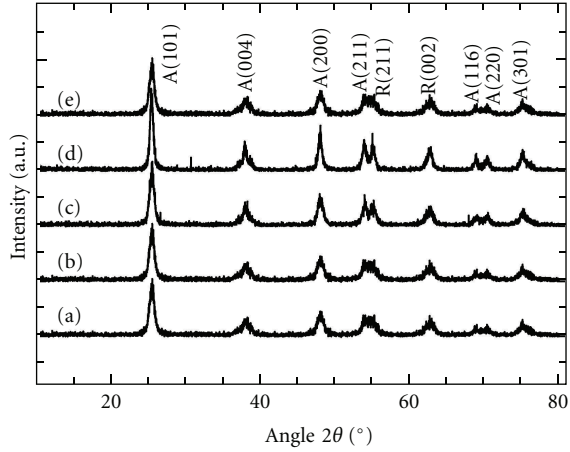


FIGURE 1: XRD patterns of TiO_2 and La-doped TiO_2 : (a) TiO_2 , (b) 0.5 wt%, (c) 0.7 wt%, (d) 1.0 wt%, and (e) 1.5 wt% La-doped TiO_2 .

TABLE 1: Physicochemical characteristic of TiO_2 and La-doped TiO_2 photocatalysts.

| Photocatalyst | Crystal size (D) nm | Lattice parameter (a) nm | Lattice parameter (c) nm | Unit cell volume (nm^3) |
|----------------------------|-------------------------|------------------------------|------------------------------|------------------------------------|
| TiO_2 | 40.10 | 0.37728 | 0.95015 | 0.1356 |
| 0.3 wt% La- TiO_2 | 33.12 | 0.37772 | 0.95069 | 0.1357 |
| 0.5 wt% La- TiO_2 | 30.56 | 0.37726 | 0.95051 | 0.1356 |
| 0.7 wt% La- TiO_2 | 21.41 | 0.37722 | 0.95031 | 0.1357 |
| 1.0 wt% La- TiO_2 | 19.87 | 0.37735 | 0.95024 | 0.1356 |
| 1.5 wt% La- TiO_2 | 19.80 | 0.37754 | 0.95075 | 0.1356 |
| Pure ZnO | 53.11 | 0.3248 | 0.5205 | 0.0476 |
| 1.0% La-ZnO | 20.58 | 0.3267 | 0.5182 | 0.0472 |

was observed that the peak at $2\theta = 25.4^\circ$ for La-doped TiO_2 photocatalysts were slightly shifted to lower angles which shows that the presence of the large radius of La^{3+} (1.15 Å) may interstitially substitutes in TiO_2 lattice rather substitute for relatively small radius Ti^{4+} (0.745 Å), and this cause, lattice distortion in La-doped TiO_2 [22]. The crystal size was calculated using Scherer's formula for the (101) plane of TiO_2 and La-doped TiO_2 photocatalysts, and the values are given in Table 1. The average grain size from the broadening of the (101) peak of anatase was 19–40 nm. The crystal size of La-doped TiO_2 decreased with increase in La content, and their crystal size was less than that of pure TiO_2 . The decrease in crystal size was due to the incorporation of La-ion into TiO_2 , which decreases the grains growth [23]. The lattice parameters of La-doped TiO_2 (Table 1) are a little smaller than the standard values of bulk TiO_2 ($a = 0.37728$ nm, $c = 0.95015$ nm). The difference in lattice parameters shows that La^{3+} is successfully incorporated into the TiO_2 lattice where it interstitially substitutes the Ti^{4+} ion sites as the ionic radius

TABLE 2: Textural properties of pure and La-doped semiconductors.

| Photocatalyst | $A_{\text{BET}}/(\text{m}^2\text{g}^{-1})$ | $V_p/(\text{cm}^3\text{g}^{-1})$ | $d_p/(\text{nm})$ |
|----------------------------|--|----------------------------------|-------------------|
| TiO_2 | 118.5 | 0.1071 | 2.718 |
| 1.0 wt% La- TiO_2 | 98.36 | 0.117 | 4.267 |
| Pure ZnO | 53.11 | 0.0942 | 1.131 |
| 1.0% La-ZnO | 39.56 | 0.1053 | 2.378 |

of La^{3+} (0.106 nm) is larger than that of Ti^{4+} (0.061 nm) [24, 25]. The shift in the peak position and the change in the lattice parameters show that La^{3+} ions are replacing the Ti^{4+} ions. Representative TEM images of La-doped TiO_2 are shown in Figure 2. Figure 2(a) reveals the uniform size of the TiO_2 nanoparticles with a few aggregations, and the average particle diameter was estimated to be about 20 nm. HRTEM image (Figure 2(b)) revealed the presence of highly crystalline TiO_2 nanoparticles in La-doped TiO_2 photocatalysts. The electron diffraction pattern of La-doped TiO_2 photocatalysts shown in Figure 2(c) further indicates that the samples were composed of highly crystalline TiO_2 nanoparticles.

3.1.2. Nitrogen Adsorption Measurements. The nitrogen adsorption-desorption isotherms of pure and La-doped TiO_2 and their textural parameters are shown in Figure 3 and Table 2, respectively. TiO_2 and La-doped TiO_2 samples exhibit adsorption isotherms similar to Type II [26]. Type II isotherm is often observed when multilayer adsorption occurs on a nonporous solid. The surface area of pure TiO_2 was about $118.5\text{ m}^2/\text{g}$ while La-doped TiO_2 exhibited a surface area of $98.36\text{ m}^2/\text{g}$. The decrease in the surface area for La-doped TiO_2 can be attributed to the partial filling of the pores in TiO_2 by La^{3+} nanoparticles. The pore diameters of pure and 1 wt% La-doped TiO_2 were 2.718 nm and 4.267 nm, respectively. The decrease in surface area and corresponding increase in average pore diameter may be due to the collapse of considerably narrow pores to form broad pores in presence of La ions. Similar trend of results were previously observed for semiconductors doped with transition metals [27]. This shows that drastic modifications of pore structures take place when semiconductor oxides are doped with transition metals, and further, the effect probably depends on the individual metal characteristics. However, this trend is not common for all metal ion-doped semiconductors. The large pore of La-doped TiO_2 also allows an easy diffusion of the pollutant molecules in and around the semiconductor, thus enhancing the adsorption of pollutant molecules and its intermediate on the surface of the photocatalysts. It is interesting to note that the surface area of TiO_2 and 1 wt% of La-doped TiO_2 are relatively higher than that of ZnO ($53.11\text{ m}^2/\text{g}$) and 1 wt% of La-doped ZnO ($39.56\text{ m}^2/\text{g}$) [18].

3.1.3. Atomic Force Microscope (AFM) and HR-SEM Analysis. The two-dimensional surface AFM images and surface roughness profiles of TiO_2 and 1 wt% La-doped TiO_2 are shown in Figures 4 and 5. From Figure 4(a), it could be

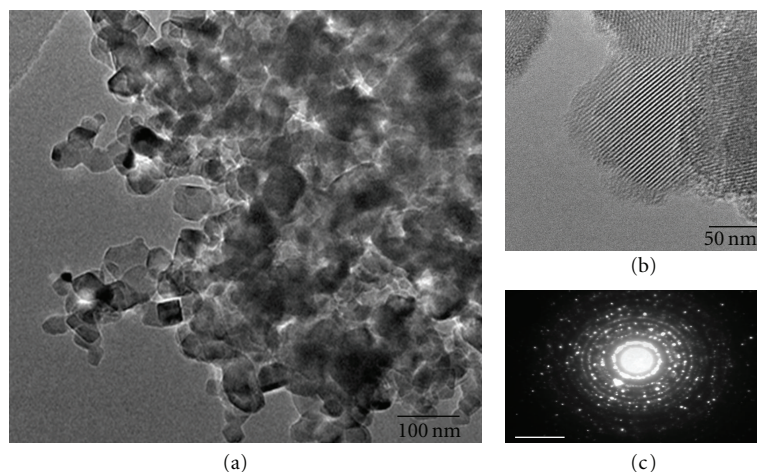


FIGURE 2: TEM images of 1.0 wt% La-doped TiO₂ (a) HR-TEM image (b) HR-TEM of the selective area, and (c) TEM image with electron diffraction pattern.

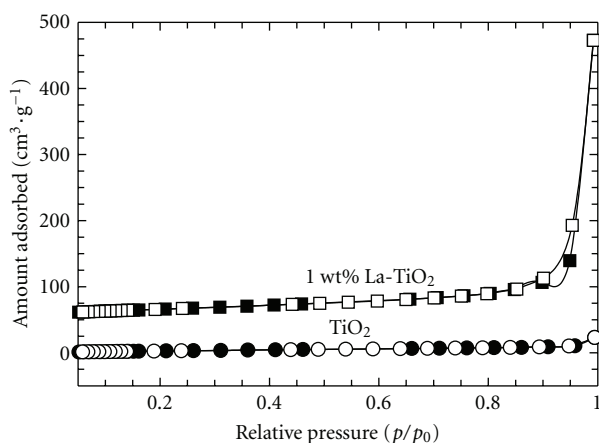


FIGURE 3: Nitrogen adsorption-desorption isotherms of TiO₂ and 1 wt% La-doped TiO₂.

observed that the size of TiO₂ was not widely distributed and the grain size was big. The average roughness value (R_{av}) of pure TiO₂ was 0.304 nm. However, for La-doped TiO₂ the grains are sharpened and their size decreased to about 50%. The average roughness value (R_{av}) increased to 0.576 nm. So we safely conclude that the incorporation of La³⁺ into the lattice of TiO₂ can control the grain growth and enhance the surface roughness of TiO₂ photocatalysts. From the surface roughness values it can be revealed that La-doped TiO₂ possesses high rough and porous surface than pure TiO₂. These high rough and porous surfaces of La-doped TiO₂ are beneficial to enhance the photocatalytic activity for the degradations of organic pollutants present in aqueous solution [28]. The high resolution-scanning electron micrographs (HR-SEM) of TiO₂ and that of 1 wt% La-doped TiO₂ are presented in Figures 6(a) and 6(b). TiO₂ particles in Figure 6(a) seem to be well separated with regular shape. The morphology of TiO₂ appears to be retained in

1 wt% La-doped TiO₂ (Figure 6(b)) with random particle size distributions.

3.1.4. X-Ray Photoelectron Spectroscopy (XPS) Analysis. Survey spectrum (Figure 7(a)) of La-doped TiO₂ photocatalyst exhibits the presence of Ti, O, and La elements. XPS spectrum of Ti-2p of TiO₂ is shown in Figure 7(b). Ti 2p peak appeared as a single, well-defined, spin-split doublet with the typical interval of 6 eV between its two peaks which corresponds to Ti⁴⁺ in a tetragonal structure (i.e., Ti 2p_{1/2} and Ti 2p_{3/2}, shown in Figure 7(b)). The binding energies of the peaks within the doublet were found to be 464.8 eV for Ti 2p_{1/2} and 459.0 eV for Ti 2p_{3/2} signal, and this was in good agreement with the binding energies of TiO₂ found in the literature [29] (464.34 eV for Ti 2p_{1/2} peak and 458.8 eV for Ti 2p_{3/2} peak). The spectrum for Ti 2p of 1 wt% La-doped TiO₂ is also shown in Figure 7(b). It carries a similar feature as that of XPS spectrum, Ti 2p of TiO₂. The XPS spectrum of O²⁻ of TiO₂ is shown in Figure 7(c). An intense signal about 531 eV due to O²⁻ ions of TiO₂ was observed. This peak was attributed to the Ti–O in TiO₂ and OH groups on the surface of the photocatalysts [30, 31]. The shoulder about 532 eV of the main O1s peak can be attributed to the presence of loosely bound oxygen of the surface-adsorbed CO₃²⁻, H₂O, or O₂ [32]. The XPS spectrum of O 1s of 1.0 wt% La-doped TiO₂ is also shown in Figure 7(c). The spectrum of O 1s broadened due to the incorporation of La³⁺ into the TiO₂ lattice. The XPS spectrum of La 3d is shown in Figure 7(d). La³⁺ ions that incorporated into TiO₂ lattice make interaction with oxidic sites of TiO₂ (Ti–O–La) and appear to provide a broadened spectrum of La 3d. A similar broad peak for La 3d spectrum of La³⁺ was also observed by Liqiang et al. [33] for La-doped TiO₂ photocatalysts. These results conclude that La elements existed mainly as +3 valence in La-doped TiO₂, Ti elements were both mainly as +4 valence, and both O elements had at least two kinds of chemical states, crystal lattice oxygen (1), and adsorbed oxygen (2). The presence of La, Ti, and O

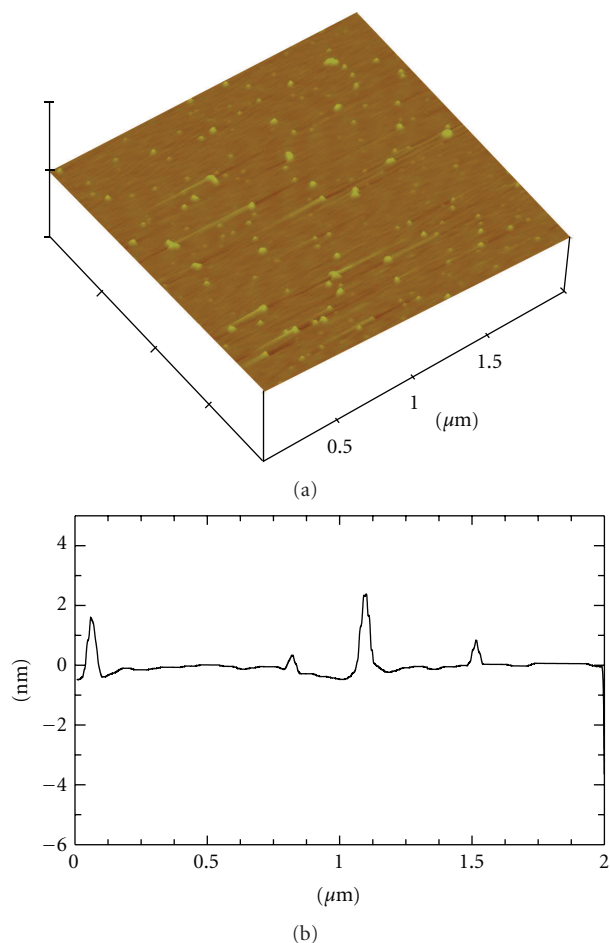


FIGURE 4: (a) AFM image and (b) surface roughness profile of TiO_2 .

elements in TiO_2 and La-doped TiO_2 is also observed from the EDX spectra (See Figures 1(a) and 1(b) in Supplementary material available on line at doi: 10.1155/2012/921412), and the results are consistent with XPS analysis.

3.2. Degradation Mechanism of La-Doped TiO_2 . To evaluate the photocatalytic activity of TiO_2 and La-doped TiO_2 a series of experiments were carried out for MCP degradation in aqueous suspension with the light of wavelengths 254 and 365 nm. The photocatalytic degradation of MCP follows a pseudo-first-order reaction. The apparent reaction rate constants (k) and $t_{1/2}$ values of TiO_2 and La-doped TiO_2 are presented in Tables 3 and 4. For comparison the rate constant and $t_{1/2}$ values of pure ZnO La-doped ZnO are also presented in Tables 3 and 4. La-doped TiO_2 showed higher rate of degradation than TiO_2 for the light of wavelength of 254 nm and 365 nm. The rate constant increased with increase in La loading up to 1.0 wt%, and with further increase in loading, the rate constant decreased. It was found that the reaction rate increased with the increase of lanthanum content (0.3–1 wt% La) at first and then declined when the cerium ion content (1.5 wt% La) exceeded its optimal value. In general, when increasing the metal ion concentration the carrier mobility decreased [34]. In the present study,

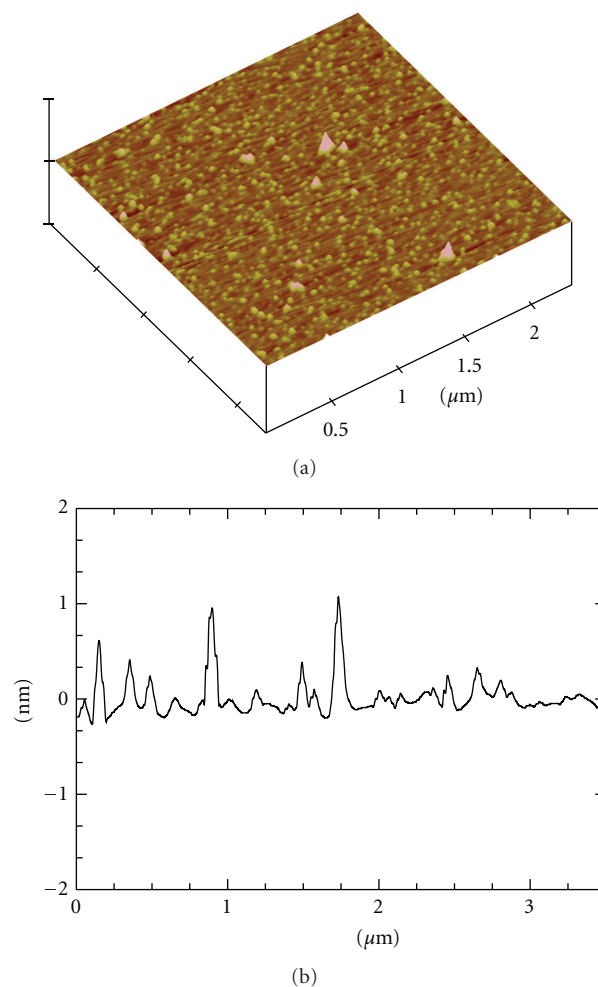


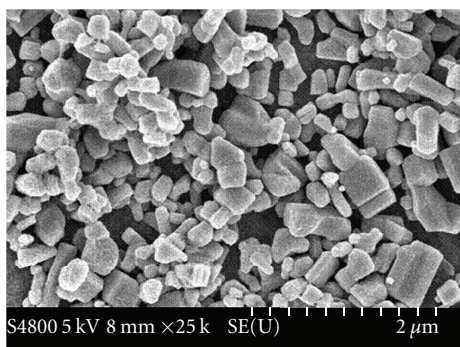
FIGURE 5: (a) AFM image and (b) surface roughness profile of 1.0 wt% La-doped TiO_2 .

the higher concentration of lanthanum in La-doped TiO_2 photocatalysts decreased its crystallinity and carrier mobility, which led to reduction of the photocatalytic activity of TiO_2 . The reasons for the enhanced photocatalytic activity of TiO_2 by the incorporation of lanthanum can be explained as follows. The incorporation of La^{3+} in the lattice of TiO_2 decreases crystallite sizes and inhibits the electron-hole recombination on excitation of La-doped TiO_2 . Moreover it increased the surface roughness and provided more active surface area for photocatalytic reaction. The introduction of La^{3+} produces lattice swelling [35] and hence increases the surface roughness of La^{3+} (0.576 nm) than Ti^{4+} (0.304 nm). Thus, the increase in roughness of La^{3+} in La-doped TiO_2 makes the structure loose and the grains activated which can be attributed to the high photocatalytic activity of TiO_2 . Further, an interesting observation was that the rate constant of 1 wt% La-doped TiO_2 was higher than that of ZnO and 1 wt% La-doped ZnO [18] (Tables 3 and 4). Smaller particle size, high porosity, and high surface roughness are the reasons for the excellent photocatalytic activity of

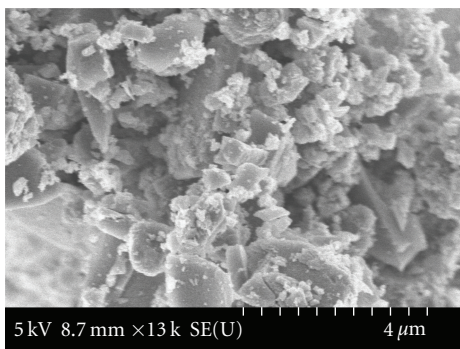
TABLE 3: Apparent reaction rate constants and $t_{1/2}$ values for the degradation of MCP with 254 nm.

| Photocatalyst | Apparent reaction rate constant k ($\times 10^{-2} \text{ min}^{-1}$) | $t_{1/2}$ values (min) | Correlation coefficient (R^2 value) |
|-----------------------------|--|------------------------|--|
| TiO ₂ | 6.0 | 11.55 | 0.985 |
| 0.3 wt% La-TiO ₂ | 8.0 | 8.66 | 0.976 |
| 0.5 wt% La-TiO ₂ | 9.5 | 7.29 | 0.981 |
| 0.7 wt% La-TiO ₂ | 12.0 | 5.76 | 0.990 |
| 1.0 wt% La-TiO ₂ | 14.0 | 4.95 | 0.982 |
| 1.5 wt% La-TiO ₂ | 11.0 | 6.3 | 0.989 |
| Pure ZnO | 5.25 | 13.20 | 0.976 |
| 1.0% La-ZnO | 8.01 | 8.65 | 0.977 |

MCP = 40 mgL⁻¹, TiO₂ or La-TiO₂ = 100 mg/100 mL, pH = 5, UV = 8 lamps, λ = 254 nm, adsorption equilibrium time = 30 min, and irradiation time = 60 min.



(a)



(b)

FIGURE 6: HR-SEM pictures of (a) TiO₂ and (b) 1.0 wt% La-doped TiO₂.

La-doped TiO₂ than ZnO and La-doped ZnO. The half-life of degradation decreased with increase in La loading up to 1.0 wt%, and with further increase of La the half-life of degradation gets increase. The half-life of degradation with 1.0 wt% La-doped TiO₂ was almost half the value of TiO₂. These results also reveal the essential role of La³⁺ in La-doped TiO₂ for the degradation of MCP.

3.3. Photocatalytic Mineralization of MCP. Mineralization of hazardous pollutants by a cost-effective process is very important for industrial applications. To study the complete

TABLE 4: Apparent reaction rate constants and $t_{1/2}$ values for the degradation of MCP with 365 nm.

| Photocatalyst | Apparent reaction rate constant k ($\times 10^{-2} \text{ min}^{-1}$) | $t_{1/2}$ values (min) | Correlation coefficient (R^2 value) |
|-----------------------------|---|------------------------|--|
| TiO ₂ | 5.3 | 13.08 | 0.999 |
| 0.3 wt% La-TiO ₂ | 5.8 | 11.95 | 0.995 |
| 0.5 wt% La-TiO ₂ | 6.7 | 10.34 | 0.993 |
| 0.7 wt% La-TiO ₂ | 8.2 | 8.45 | 0.994 |
| 1.0 wt% La-TiO ₂ | 9.0 | 7.7 | 0.985 |
| 1.5 wt% La-TiO ₂ | 8.6 | 8.06 | 0.989 |
| Pure ZnO | 3.00 | 13.20 | 0.999 |
| 1.0% La-ZnO | 8.00 | 8.66 | 0.985 |

MCP = 40 mgL⁻¹, TiO₂ or La-TiO₂ = 100 mg/100 mL, pH = 5, UV = 8 lamps, λ = 365 nm, adsorption equilibrium time = 30 min, and irradiation time = 60 min.

mineralization of MCP, the degradation was carried out with either TiO₂ or La-doped TiO₂ photocatalysts. The plot of total organic carbon value of MCP with time is illustrated in Figures 8 and 9 for the light of wavelength 254 nm and 365 nm, respectively. For comparison the mineralization results of pure ZnO and la-doped ZnO are also presented in Figures 8 and 9. It can be clearly seen from Figures 8 and 9 that the decrease of TOC concentration of MCP for La-doped TiO₂ was relatively higher compared to pure TiO₂. Decrease of TOC value of MCP showed maximum for 1 wt% La-doped TiO₂ and achieved complete mineralization (100% TOC removal) of MCP within 3 h, whereas only 30% TOC removal was observed for pure TiO₂ over the same period of irradiation time. Rapid mineralization of MCP over La-doped TiO₂ can be associated with the suppression of electron-hole recombination by La³⁺ in the lattice of TiO₂ and generation of more number of $\cdot\text{OH}$ radicals by oxidation of holes. $\cdot\text{OH}$ radicals are the primary oxidizing species which break down organic pollutants into a variety of intermediate products on the way to total mineralization to carbon dioxide and harmless inorganic ions [36]. The results demonstrated that 1.0 wt% La-doped TiO₂ was found

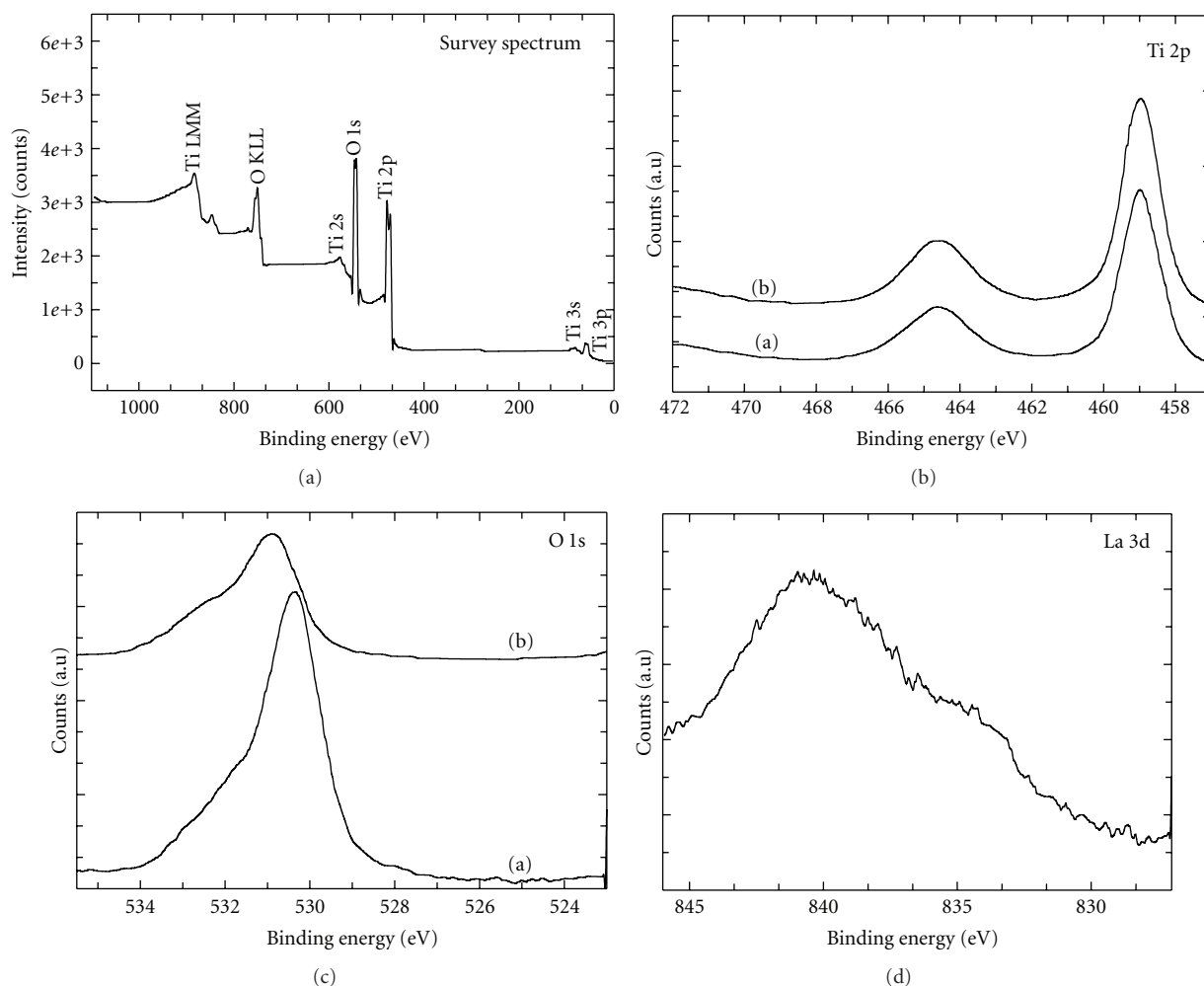


FIGURE 7: XPS spectra of pure and 1.0 wt% La-doped TiO_2 : (a) survey spectrum of TiO_2 (b) Ti 2p (a = TiO_2 ; b = 1.0 wt% La- TiO_2) (c) O 1s (a = TiO_2 ; b = 1.0 wt% La- TiO_2), and (d) La 3d.

to be more active than other photocatalysts, namely, pure TiO_2 , 0.3 wt%, 0.5 wt%, 0.7 wt%, and 1.5 wt% La-doped TiO_2 and those photocatalysts exhibited TOC removal of 30%, 28%, 75%, 70%, 75%, 87%, and 90%, respectively. 1.0 wt% La-doped TiO_2 required shorter irradiation time for the complete mineralization of MCP compared to previously reported photocatalysts (pure ZnO, 1.0 wt% La-doped ZnO), and they disclosed only 28% and 70% TOC removal of MCP within 3 h, under the same experimental conditions [20]. Small particle size, high surface area, high surface roughness and porous surface of La-doped TiO_2 , and the suppression of electron-hole recombination by La^{3+} were the reasons for the high photocatalytic activity of La-doped TiO_2 than other photocatalysts.

3.4. Relative Photonic Efficiency. The concept of relative photonic efficiency (ξ_r) affords comparison of catalyst efficiencies for the photocatalytic degradation of organic pollutants. To evaluate ξ_r , photocatalytic degradation of MCP was carried out over TiO_2 (Degussa P-25) or La-doped TiO_2 or other photocatalysts (ZnO and 1 wt% La-doped ZnO) with

the lights of wavelengths 254 and 365 nm, and the results are presented in Table 5. The relative photonic efficiencies of La-doped TiO_2 photocatalysts were greater than TiO_2 and this revealed the effectiveness of metal-doped systems. The relative photonic efficiencies of light of wavelength 254 nm for La-doped TiO_2 are greater than light of wavelength 365 nm. The results were in good agreement with degradation and mineralization studies. Comparing the high efficiency of La-doped TiO_2 photocatalysts with standard catalyst (Degussa P-25), 1.0 wt% La-doped TiO_2 is about 2.3 and 1.8 times more efficient than Degussa P-25 for the light of wavelength 254 nm and 365 nm, respectively. While comparing with La-doped ZnO photocatalysts, La-doped TiO_2 was about 1.54 and 1.46 times higher for the light of wavelength 254 nm and 365 nm, respectively. The relative photonic efficiency of La-doped TiO_2 photocatalysts was compared with already reported photocatalysts [21], and the values are shown in Table 5. 1 wt% La-doped TiO_2 (254 nm) photocatalyst was about 6.13 times more efficient than Baker and Adamson whereas 9.32 times higher than Hombikat UV-100. Further, the relative photonic efficiency

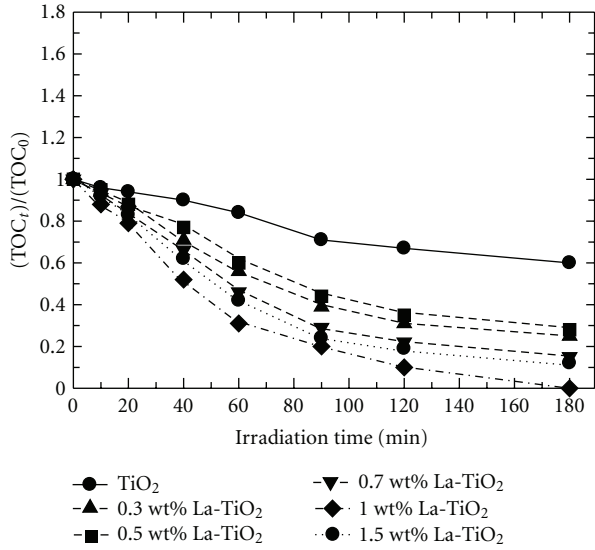
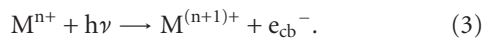
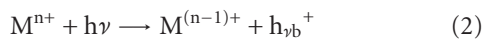
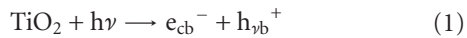


FIGURE 8: Comparison of photocatalytic mineralization of MCP using TiO_2 and La-doped TiO_2 photocatalysts. (MCP concentration = 40 mg L^{-1} ; catalyst amount = $100 \text{ mg}/100 \text{ mL}$; solution pH = 5; $\lambda = 254 \text{ nm}$).

of 1 wt% La-doped TiO_2 (254 nm) was relatively higher than the values reported for other commercial photocatalysts (Tioxide, Sargent-Weich and Fluka AG). It may be presumed that the incorporation of La^{3+} in the lattice of TiO_2 greatly enhance the photocatalytic performance of TiO_2 and hence showed high relative photonic efficiency value than all other photocatalysts.

3.5. Photocatalytic Reaction Mechanism. Metal ions doped on the semiconductors have been shown to improve the photocatalytic electron-transfer processes at the semiconductor interface [9, 37–39]. For example, the deposition of Au on TiO_2 led to improvement in the efficiency of photocatalytic oxidation of thiocyanate ions [40]. Doped metal ions influence the photocatalytic activity of TiO_2 by acting as electron (or hole) traps and by altering e^-/h^+ pair recombination rate through the following processes:

Charge pair generation



Charge trapping

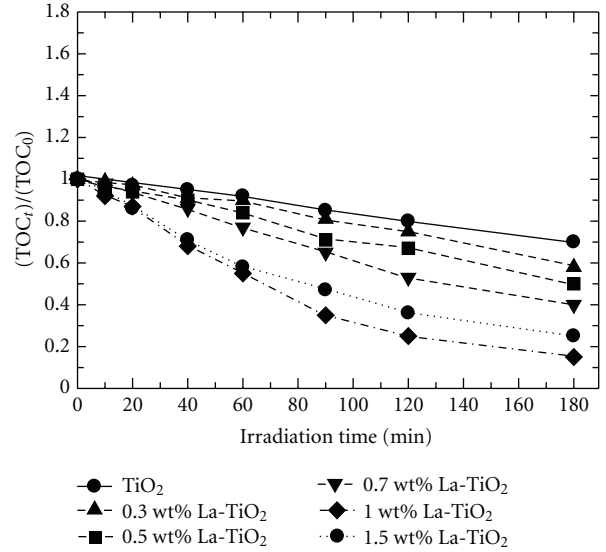
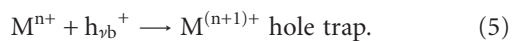
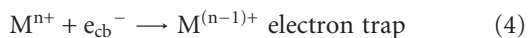
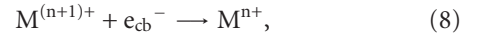
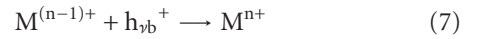
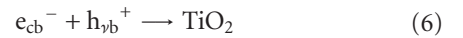


FIGURE 9: Comparison of photocatalytic mineralization of MCP using TiO_2 and La-doped TiO_2 photocatalysts. (MCP concentration = 40 mg L^{-1} ; catalyst amount = $100 \text{ mg}/100 \text{ mL}$; solution pH = 5; $\lambda = 365 \text{ nm}$).

Recombination



where M^{n+} is a metal ion dopant. The energy level for $\text{M}^{n+}/\text{M}^{(n-1)+}$ lies below the conduction band edge (E_{cb}) and the energy level for $\text{M}^{n+}/\text{M}^{(n+1)+}$ above the valence band edge (E_{vb}). In the present study, photocatalytic reaction mechanism for the degradation of MCP over La-doped semiconductor is speculated as follows. Under light illumination, La-doped TiO_2 photocatalysts are exposed, and the electrons are excited from the valence band state to conduction band state. Liqiang et al. [33] demonstrated that surface oxygen vacancies and defects states by La doping could be favorable in capturing the photoinduced electrons during the process of photocatalytic reactions. Previously Chen et al. [41] reported that the introduction of new impurity states due to the incorporation of La^{3+} decreases the recombination of photogenerated electrons and holes. Hence, in the present study, we believe that the excited electrons in the conduction band transfer to the La^{3+} states, and the holes present in the valence band are available for the photocatalytic oxidation of MCP. The rare earth metal (here, La), which usually act as a reservoir for photogenerated electrons, promotes an efficient charge separation in La-doped TiO_2 photocatalysts. In addition, small particle size, high surface area, high surface roughness, and porous surface of La-doped TiO_2 were also the reason for the high photocatalytic activity of La-doped TiO_2 .

TABLE 5: Comparison of relative photonic efficiencies in the photocatalytic degradation of MCP by pure and La-doped semiconductors (TiO₂ and ZnO).

| Photocatalyst | Relative photonic efficiency (ξ_r) | |
|--------------------------------------|--|---------------|
| TiO ₂ | 1.0 ± 0.01 | In this study |
| 1.0 wt% La-TiO ₂ (254 nm) | 2.33 ± 0.01 | In this study |
| 1.0 wt% La-TiO ₂ (365 nm) | 1.82 ± 0.01 | In this study |
| Pure ZnO | 1.03 ± 0.01 | [18] |
| 1.0% La-ZnO (254 nm) | 1.51 ± 0.01 | [18] |
| Baker and Adamson | 0.38 ± 0.02 | [18] |
| Tioxide | 1.9 ± 0.1 | [21] |
| Sargent-Welch | 2.1 ± 0.1 | [21] |
| Fluka AG | 2.2 ± 0.2 | [21] |
| Hombikat UV-100 | 0.25 ± 0.02 | [21] |

MCP = 40 mg L⁻¹, TiO₂ or La-TiO₂ = 100 mg/100 mL, pH = 5, UV = 8 lamps, λ = 254/365 nm, adsorption equilibrium time = 30 min, and irradiation time = 60 min.

4. Conclusion

Highly efficient photocatalyst, La-doped TiO₂, was successfully synthesized and characterized by various sophisticated techniques. XRD and TEM analysis revealed the presence of highly crystalline TiO₂ nanoparticles. AFM results demonstrated that La-doped photocatalysts have rough and highly porous surface, which is a critical parameter to enhance the photocatalytic activity. The photocatalytic activity of La-doped TiO₂ in the degradation of MCP was studied, and the results were compared with degradation results of La-doped ZnO photocatalysts. La-doped TiO₂ photocatalysts were found to be very active, and its rate constant was 1.75 and 1.125 times higher than La-doped ZnO photocatalysts for the light of wavelength 254 nm and 365 nm, respectively. The relative photonic efficiency of La-doped TiO₂ catalyst was relatively higher than that of previously reported and some of the commercial photocatalysts. Small particle size, high surface area, high surface roughness, and the suppression of electron-hole recombination by La³⁺ were the reasons for the high photocatalytic activity of La-doped TiO₂ for the removal of MCP than other photocatalysts. It is concluded that incorporation of rare earth metal into the semiconductors has been proven to be a promising approach to improve the photocatalytic activity of semiconductors.

Acknowledgment

The authors acknowledge the Ministry of Education, Culture, Sports, Science and Technology (MEXT) for the funding through "High-Tech Research Center" a project for private universities, 2004–2008.

References

- [1] N. Serpone and E. Pelizzetti, *Photocatalysis: Fundamentals and Applications*, John Wiley & Sons, New York, NY, USA, 1989.

- [2] M. R. Hoffmann, S. T. Martin, W. Choi, and D. W. Bahnemann, "Environmental applications of semiconductor photocatalysis," *Chemical Reviews*, vol. 95, no. 1, pp. 69–96, 1995.
- [3] A. Fujishima, T. N. Rao, and D. A. Tryk, "Titanium dioxide photocatalysis," *Journal of Photochemistry and Photobiology C: Photochemistry Reviews*, vol. 1, pp. 1–21, 2000.
- [4] Z. Zou, J. Ye, K. Sayama, and H. Arakawa, "Direct splitting of water under visible light irradiation with an oxide semiconductor photocatalyst," *Nature*, vol. 414, no. 6864, pp. 625–627, 2002.
- [5] Y. Wang, Y. Hao, H. Cheng et al., "Photoelectrochemistry of transition metal-ion-doped TiO₂ nanocrystalline electrodes and higher solar cell conversion efficiency based on Zn²⁺-doped TiO₂ electrode," *Journal of Materials Research*, vol. 34, no. 12, pp. 2773–2779, 1999.
- [6] P. Yang, C. Lu, N. P. Hua, and Y. K. Du, "Titanium dioxide nanoparticles co-doped with Fe³⁺ and Eu³⁺ ions for photocatalysis," *Materials Letters*, vol. 57, no. 8, pp. 794–801, 2002.
- [7] J. Moon, H. Takagi, Y. Fujishiro, and M. Awano, "Preparation and characterization of the Sb-doped TiO₂ photocatalysts," *Journal of Materials Science*, vol. 36, no. 4, pp. 949–955, 2001.
- [8] R. Asahi, T. Morikawa, T. Ohwaki, K. Aoki, and Y. Taga, "Visible-light photocatalysis in nitrogen-doped titanium oxides," *Science*, vol. 293, no. 5528, pp. 269–271, 2001.
- [9] W. Choi, A. Termin, and M. R. Hoffmann, "The role of metal ion dopants in quantum-sized TiO₂: correlation between photoreactivity and charge carrier recombination dynamics," *Journal of Physical Chemistry*, vol. 98, no. 51, pp. 13669–13679, 1994.
- [10] Y. Zhang, M. Wang, and J. Xu, "The synthesis and characterization of picolinic acid: Eu³⁺ complex in SiO₂ xerogels and energy transfer from picolinic acid to Eu³⁺," *Materials Science and Engineering: B*, vol. 47, p. 23, 1997.
- [11] S. T. Selvan, T. Hayakawa, and M. Nogami, "Remarkable influence of silver islands on the enhancement of fluorescence from Eu³⁺ ion-doped silica gels," *Journal of Physical Chemistry B*, vol. 103, no. 34, pp. 7064–7067, 1999.
- [12] M.-H. Lee, S.-G. Oh, and S.-C. Yi, "Preparation of Eu-doped Y₂O₃ luminescent nanoparticles in nonionic reverse microemulsions," *Journal of Colloid and Interface Science*, vol. 226, no. 1, pp. 65–70, 2000.
- [13] A. Kurita, T. Kushida, T. Izumitani, and M. Matsukawa, "Room-temperature persistent spectral hole burning in Sm²⁺-doped fluoride glasses," *Optics Letters*, vol. 19, no. 5, pp. 314–316, 1994.
- [14] Th. Schmidt, R. M. MacFarlane, and S. Völker, "Persistent and transient spectral hole burning in Pr³⁺- and Eu³⁺-doped silicate glasses," *Physical Review B*, vol. 50, no. 21, pp. 15707–15718, 1994.
- [15] K. Fujita, K. Hirao, K. Tanaka, N. Soga, and H. Sasaki, "Persistent spectral hole burning of Eu³⁺ ions in sodium aluminosilicate glasses," *Journal of Applied Physics*, vol. 82, no. 10, pp. 5114–5120, 1997.
- [16] H. Yoshioka and S. Kikkawa, "Oxide ion conduction in A-site deficient La-Ti-Al-O perovskite," *Journal of Materials Chemistry*, vol. 8, no. 8, pp. 1821–1826, 1998.
- [17] I. Atribak, I. S. Basañez, A. B. López, and A. García García, "Catalytic activity of La-modified TiO₂ for soot oxidation by O₂," *Catalysis Communications*, vol. 8, no. 3, pp. 478–482, 2007.
- [18] S. Anandan, A. Vinu, K. L. P. S. Lovely et al., "Photocatalytic activity of La-doped ZnO for the degradation of monocrotophos in aqueous suspension," *Journal of Molecular Catalysis A: Chemical*, vol. 266, no. 1-2, pp. 149–157, 2007.

- [19] Y. Ohko, K. I. Iuchi, C. Niwa et al., "17 β -estradiol degradation by TiO₂ photocatalysis as a means of reducing estrogenic activity," *Environmental Science and Technology*, vol. 36, no. 19, pp. 4175–4181, 2002.
- [20] M. V. Shankar, S. Anandan, N. Venkatachalam, B. Arabindoo, and V. Murugesan, "Fine route for an efficient removal of 2,4-dichlorophenoxyacetic acid (2,4-D) by zeolite-supported TiO₂," *Chemosphere*, vol. 63, no. 6, pp. 1014–1021, 2006.
- [21] N. Serpone and A. Salinaro, "Terminology, relative photonic efficiencies and quantum yields in heterogeneous photocatalysis. Part I: suggested protocol," *Pure and Applied Chemistry*, vol. 71, no. 2, pp. 303–320, 1999.
- [22] R. D. Shannon, "Revised effective ionic radii and systematic studies of interatomic distances in halides and chalcogenides," *Acta Crystallographica Section A. Crystal Physics, Diffraction, Theoretical and General Crystallography*, vol. 32, pp. 751–767, 1976.
- [23] J. Lin and J. C. Yu, "An investigation on photocatalytic activities of mixed TiO₂-rare earth oxides for the oxidation of acetone in air," *Journal of Photochemistry and Photobiology A: Chemistry*, vol. 116, no. 1, pp. 63–67, 1998.
- [24] J. A. Dean, *Lange's Handbook of Chemistry*, McGraw-Hill, New York, NY, USA, 15th edition, 1999.
- [25] C. P. Sibin, S. R. Kumar, P. Mukundan, and K. G. Warrier, "Structural modifications and associated properties of lanthanum oxide doped sol-gel nanosized titanium oxide," *Chemistry of Materials*, vol. 14, no. 7, pp. 2876–2881, 2002.
- [26] K. S. W. Singh, D. H. Everett, R. A. W. Haul et al., "Reporting physisorption data for gas/solid systems with special reference to the determination of surface area and porosity," *Pure and Applied Chemistry*, vol. 57, no. 4, pp. 603–619, 1985.
- [27] D. Das, H. K. Mishra, A. K. Dalai, and K. M. Parida, "Iron, and manganese doped SO₄²⁻/ZrO₂-TiO₂ mixed oxide catalysts: studies on acidity and benzene isopropylation activity," *Catalysis Letters*, vol. 93, no. 3-4, pp. 185–193, 2004.
- [28] M. O. Abou-Helal and W. T. Seeber, "Preparation of TiO₂ thin films by spray pyrolysis to be used as a photocatalyst," *Applied Surface Science*, vol. 195, no. 1–4, pp. 53–62, 2002.
- [29] J. F. Moulder, W. F. Stickle, P. E. Sobol, and K. D. Bomben, *Handbook of X-Ray Photoelectron Spectroscopy*, Physical Electronics Division/Perkin-Elmer, Eden Prairie, Minn, USA, 1992.
- [30] L. Wu, J. C. Yu, L. Z. Zhang, X. C. Wang, and W. K. Ho, "Preparation of a highly active nanocrystalline TiO₂ photocatalyst from titanium oxo cluster precursor," *Journal of Solid State Chemistry*, vol. 177, no. 7, pp. 2584–2590, 2004.
- [31] J. C. Yu, J. G. Yu, H. Y. Tang, and L. Z. Zhang, "Effect of surface microstructure on the photoinduced hydrophilicity of porous TiO₂ thin films," *Journal of Materials Chemistry*, vol. 12, no. 1, pp. 81–85, 2002.
- [32] M. N. Islam, T. B. Ghosh, K. L. Chopra, and H. N. Acharya, "XPS and X-ray diffraction studies of aluminum-doped zinc oxide transparent conducting films," *Thin Solid Films*, vol. 280, no. 1-2, pp. 20–25, 1996.
- [33] J. Liqiang, S. Xiaojun, X. Baifu, W. Baiqi, C. Weimin, and F. Honggang, "The preparation and characterization of La doped TiO₂ nanoparticles and their photocatalytic activity," *Journal of Solid State Chemistry*, vol. 177, no. 10, pp. 3375–3382, 2004.
- [34] K. L. Frindell, J. Tang, J. H. Harreld, and G. D. Stucky, "Enhanced mesostructural order and changes to optical and electrochemical properties induced by the addition of cerium(III) to mesoporous titania thin films," *Chemistry of Materials*, vol. 16, no. 18, pp. 3524–3532, 2004.
- [35] T. Sato and Y. Fukugami, "Synthesis and photocatalytic properties of TiO₂ and Pt pillared HCa₂Nb₃O₁₀ doped with various rare earth ions," *Solid State Ionics*, vol. 141-142, pp. 397–405, 2001.
- [36] R. Terzian, N. Serpone, and M. A. Fox, "Primary radicals in the photo-oxidation of aromatics—reactions of xylenols with $^{\bullet}OH$, $N@3^{\bullet}$ and H^{\bullet} radicals and formation and characterization of dimethylphenoxy, dihydroxydimethylcyclohexadienyl and hydroxydimethylcyclohexadienyl radicals by pulse radiolysis," *Journal of Photochemistry and Photobiology, A: Chemistry*, vol. 90, no. 2-3, pp. 125–135, 1995.
- [37] V. Subramanian, E. Wolf, and P. V. Kamat, "Semiconductor-metal composite nanostructures. To what extent do metal nanoparticles improve the photocatalytic activity of TiO₂ films?" *Journal of Physical Chemistry B*, vol. 105, no. 46, pp. 11439–11446, 2001.
- [38] L. Zang, C. Lange, I. Abraham, S. Storck, W. F. Maier, and H. Kisch, "Amorphous microporous titania modified with platinum(IV) chloride—a new type of hybrid photocatalyst for visible light detoxification," *Journal of Physical Chemistry B*, vol. 102, no. 52, pp. 10765–10771, 1998.
- [39] A. Heller, "Optically transparent metallic catalysts on semiconductors," *Pure and Applied Chemistry*, vol. 58, no. 9, pp. 1189–1192, 1986.
- [40] A. Dawson and P. V. Kamat, "Semiconductor-metal nanocomposites. Photoinduced fusion and photocatalysis of gold-capped TiO₂ (TiO₂/Gold) nanoparticles," *Journal of Physical Chemistry B*, vol. 105, no. 5, pp. 960–966, 2001.
- [41] W. Chen, D. Hua, T. J. Ying, and Z. J. Mei, "Photocatalytic activity enhancing for TiO₂ photocatalyst by doping with La," *Transactions of Nonferrous Metals Society of China*, vol. 16, pp. s728–s731, 2006.



Hindawi

Submit your manuscripts at
<http://www.hindawi.com>

